Soil Dynamics and Earthquake Engineering 110 (2018) 1–12

Contents lists available at ScienceDirect

Soil Dynamics and Earthquake Engineering

journal homepage: www.elsevier.com/locate/soildyn

Dynamic responses of subgrade under double-line high-speed railway

Jin Chen, Ying Zhou*

State Key Laboratory of Disaster Reduction in Civil Engineering, Tongji University, Shanghai 200092, China

ARTICLE INFO

Keywords:
High-speed railway
Subgrade
Finite element analysis
Dynamic response
Stress distribution

ABSTRACT

The majority of high-speed railways around the world is in China and more than 90% of the high-speed railways in China are double-line. At present, studies on the dynamic responses of subgrade under double-line high-speed railways are quite limited due to the complexity of these railways. In this study, a three-dimensional finite element model was developed using ABAQUS software for a double-line ballastless track-subgrade system subject to 8-carriage moving constant loads. The dynamic responses (specifically the vertical stress, displacement, velocity and acceleration) were determined at three points on the subgrade surface (Point A, Point B, and Point C) for trains travelling at different speeds (250, 300, and 360 km/h) and line patterns (unidirectional and bidirectional operations). The vertical stress distributions at selected points on the subgrade surface at these train speeds and line patterns are presented, and the vertical stress distributions along the soil depth of the subgrade at Point A and Point B are discussed. The key findings of this study are as follows. The maximum vertical displacement at the three observation points decreases as the train speed increases whereas the absolute maximum vertical velocity slightly increases as the train speed increases. In bidirectional operation, the maximum vertical stresses occur under the rails on the subgrade surface and the stress distributions are asymmetric. At Point A (point on the subgrade surface underneath the left rail in the left line), the vertical stress decreases along the soil depth and the vertical stress attenuation is more pronounced for bidirectional operation. However, at Point B (point at the centre of the subgrade surface), the vertical stress increases along the soil depth. The vertical stresses at Point A and Point B tend to be close to one another with an increase in soil depth such that the values are nearly coincident in the embankment layer within the range of train speeds investigated in this study.

1. Introduction

Nowadays, there is a great interest in the construction of high-speed railways worldwide, and high-speed railways have been built to connect major cities in countries in Asia and Europe, making travelling easier for passengers. While high-speed trains enable passengers to arrive at their destination faster, the high speeds also lead to several problems in the sub-systems of high-speed railways, which will threaten passenger safety. This is indeed evident from the statistics of accidents that occur on high-speed railways. In 1998, the Inter City Express (ICE) derailed near the village of Eschede, Germany, due to fatigue fracture of the double hub wheel of the high-speed train under dynamic loads. In 2000, two pairs of wheels of a Eurostar high-speed train travelling at full speed (300 km/h) derailed because of the uneven subgrade, resulting in 14 casualties. In 2004, a brand-new high-speed train was overthrown in Turkey as a result of derailment, which is likely because the old rail was not suitable for the new high-speed train. In 2013 and 2015, an AVE Talgo high-speed train and a TGV high-speed test train derailed as the trains sped around the corner. All of these train accidents indicate that it is crucial to investigate the performance of high-speed railway systems (i.e. train, track, and subgrade) under dynamic loads.

At present, the main models of high-speed trains comprise the Shinkansen series (Japan), TGV series (France), Eurostar series (United Kingdom), ICE series (Germany), AVE series (Spain), and CRH series (China) with axle loads ranging from 11.3 to 20 t. There are two types of track structure: (1) ballasted track and (2) ballastless track. Ballastless tracks provide smoother, comfortable ride, superior durability, and lower maintenance compared with conventional ballasted tracks. Therefore, ballastless tracks are typically used for high-speed railways with train speeds of 250 km/h and above. Subgrade is the subsystem of high-speed railways with a relatively small stiffness and it serves as the foundation for the train and track structure. The stress distributions of the subgrade structure subject to dynamic loads (particularly, high-speed dynamic loads) are intrinsically complex. The safety of high-speed railway systems will be greatly affected if the dynamic responses of the subgrade structure exceed permissible limits.

Studies on the dynamic responses of subgrade structures can be

* Corresponding author.
E-mail address: yingzhou@tongji.edu.cn (Y. Zhou).

https://doi.org/10.1016/j.soildyn.2018.03.028
Received 30 August 2017; Received in revised form 23 March 2018; Accepted 26 March 2018

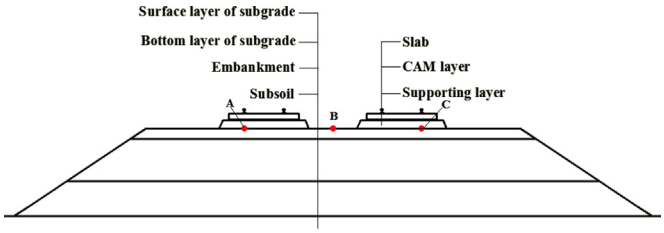

Fig. 1. Cross section of the Beijing-Shanghai double-line low-embankment high-speed ballastless slab track railway.

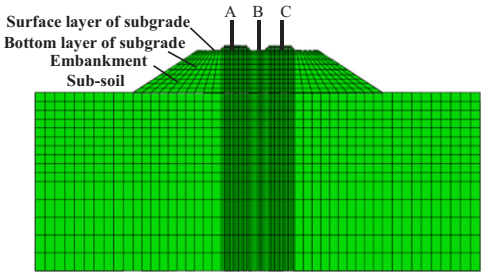

Fig. 2. FE model of the double-line ballastless track-subgrade structure.

Table 1
Key simulation parameters of the ballastless track-subgrade structure.

Type	E (MPa)	μ	Density (kg/m^3)	Internal friction angle (°)	Cohesive strength (kPa)
Rail	210,000	0.3	7800		
Slab	35,000	0.16	3000		
CAM layer	92	0.4	2000		
Supporting layer	30,000	0.16	2700		
Surface layer of subgrade	400	0.3	2400	35	70
Bottom layer of subgrade	250	0.3	1920	32	60
Embankment layer	250	0.3	1900	28	50
Ground	40	0.3	1800	25	30

Table 2
Simulation cases.

Case	Line pattern	Graphical representation	Train speed (km/h)
1	Unidirectional operation	Single-line	250
2	Bidirectional operation	Double-line	250
3	Unidirectional operation	Single-line	300
4	Bidirectional operation	Double-line	300
5	Unidirectional operation	Single-line	360
6	Bidirectional operation	Double-line	360

divided into three categories: (1) theoretical studies, (2) experimental studies, and (3) numerical simulations. Theoretical studies are focused on the development of different subgrade models using analytical methods. In earlier theoretical studies, the entire subgrade structure was treated as an elastic half-space body.

Jones et al. [1] used the dynamic stiffness matrix method to investigate the attenuation of ground vibrations, where the ground was modelled as an elastic half-space body. Krylov [2] adopted the Green function method to study the effect of train speed on the ground dynamic response. Dieterman et al. [3] determined the equivalent stiffness of an elastic half-space body (sub-soil) using Fourier transform in the spatial and temporal domains and the results showed that the critical velocity results in resonance. Grundmann et al. [4] defined the sub-soil as a layered half-space body and analysed its dynamic response

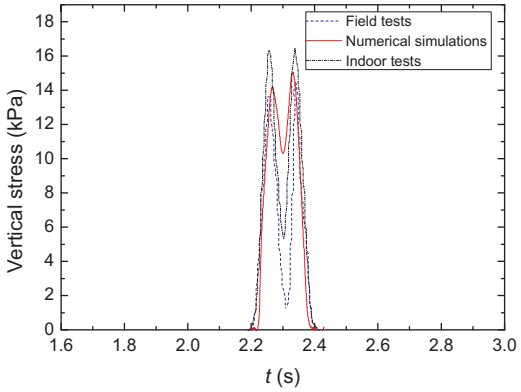

Fig. 3. Vertical stress-time history curves at Point A.

using the wavelet transformation method.

Due to the fact that the actual soil is not a completely elastic material, the elastic half-space model is gradually superseded by the viscoelastic foundation model. Hung et al. [5] studied the dynamic response of viscoelastic ground subjected to dynamic loads by using the Helmholtz potential and Fourier transform method. Alshaikh *et al.* [6] obtained the stress-time history curves at various locations using a two-dimensional layered viscoelastic model developed using Fourier transform with the method of characteristics. Bitzenbauer et al. [7] developed a layered viscoelastic subgrade model and studied its dynamic response using the Fourier transform method.

The emergence of coupling models have enabled researchers to obtain more accurate results on the dynamic responses of subgrades. Kaynia et al. [8] developed a track-ground coupling model, where a viscoelastic beam was used to simulate the embankment. The dynamic response of the subgrade was analysed based on the discontinuous stiffness matrix of the soil and the substructure principle. Takemiya et al. [9] developed a track-ground coupling model and studied its dynamic response using fast Fourier transform (FFT) and the results showed that the ground dynamic response was solely related to the characteristics of the vibration source. Sheng et al. [10] developed a vehicle-track-ground model and analysed the ground vibrations at various train speeds using Fourier transform.

With advances in experimental methods over the years, field tests and indoor physical model tests have become an indispensable means to investigate the dynamic responses of subgrade. Experimental techniques have advanced from low speeds to high speeds, ballasted tracks to ballastless tracks, and small-scale to large-scale models.

Tests have been carried out to determine the dynamic stresses of subgrade of an existing railway renovation project in Germany [11] and the results showed that the mean dynamic stress is significantly lower for the subgrade under ballastless track compared with that for the subgrade under ballasted track. Okumura et al. [12] analysed the test data of a Japanese railway line and concluded that the vehicle speed, vehicle length, and track structure have significant effects on the dynamic responses of subgrade. Madshus et al. [13,14] completed tests of a Norway-Sweden high-speed railway located on soft ground and proposed a subgrade vibration model. The Norwegian Geotechnical Institute conducted dynamic tests of Norway's first high-speed railway [15] and proved that the low-frequency peak is related to the subgrade stiffness. The Swedish National Railway Administration conducted experiments to study the dynamic response of subgrade subjected to X-2000 high-speed train loads at Ledsgard, Sweden [16,17] and the results showed that soft soil causes severe ground vibrations.

Researchers have also performed indoor physical model tests to study the dynamic responses of subgrade. Momoya et al. [18] conducted tests on a 1:5 scale ballasted track-subgrade model at low speeds and they highlighted that it is crucial to study the deformation of railway subgrade subjected to moving loads. Brown et al. [19]

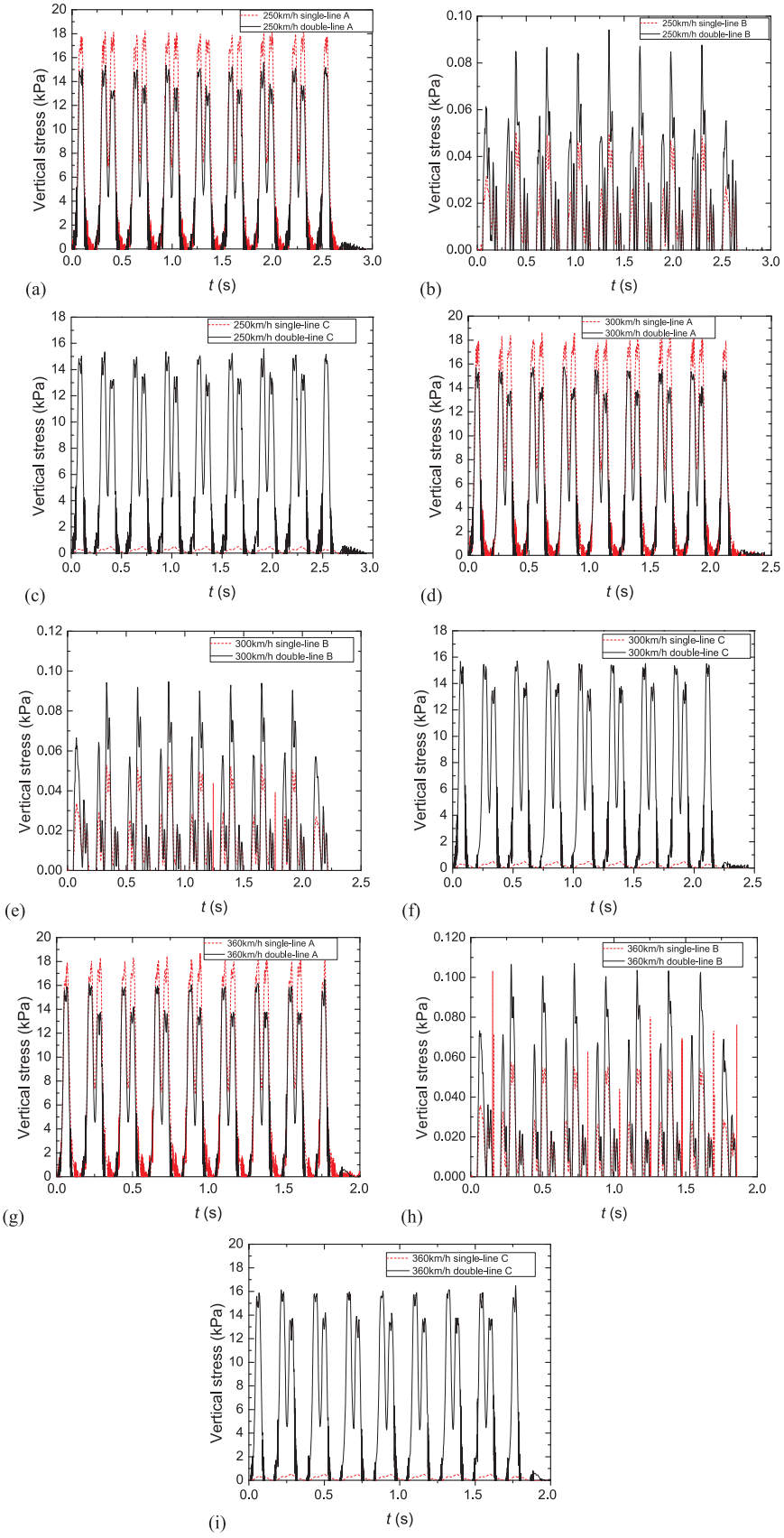

Fig. 4. Vertical stress-time history curves at Point A, Point B, and Point C.

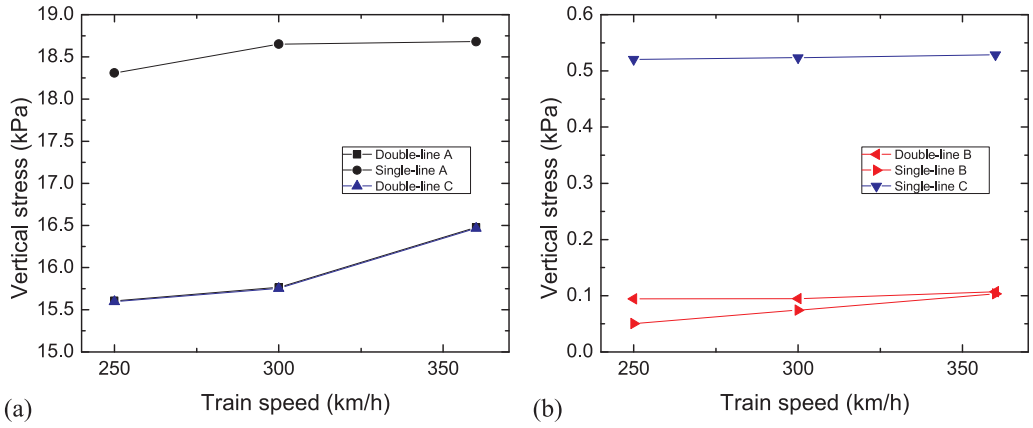

Fig. 5. Variation of the maximum vertical stress with train speed.

constructed the Nottingham railway test facility to investigate the dynamic performance of subgrade under a ballasted track subjected to train loads. Al Shaer et al. [20] constructed a 1:3 scale ballasted track-subgrade model with load M waveforms and analysed the effect of train speed and loading time on the dynamic response of subgrade. According to Ishikawa et al. [21], the moving loads result in larger subgrade deformation compared with fixed-point load for the 1:5 scale ballasted track indoor physical model. Jiang et al. [22] constructed a full-scale indoor ballastless track-subgrade model for high-speed railway, which is capable of simulating high-speed train loads. They studied the dynamic response of the subgrade at various speeds, loads, and water levels.

In general, it is particularly challenging to obtain analytical solutions in theoretical studies whereas experimental studies require high investment costs due to the need to procure materials and construct scaled models and test facilities. Due to advances in computer technology and numerical methods, numerical simulations provide a feasible means to obtain highly precise solutions and have become an important research methodology that complements analytical and experimental methods. A large number of numerical models have been proposed to investigate the subgrade or ground behaviour subjected to train loads.

Due to limitations in computer technology in the past, only two-dimensional (2D) models were developed to investigate train-induced vibrations [23]. For instance, Takemiya et al. [24] analysed ground transient response induced by uniform strip loads for different railway track structures using a 2D track-ground model. Ekevid et al. [25] proposed a 2D finite element (FE) model to study wave propagation in the ground and the results showed that high train speeds may result in high vibration levels.

A computationally-efficient 2.5D FE model was later proposed to simulate the dynamic responses of subgrade and ground subjected to train loads [26]. Yang et al. [27,28] developed a 2.5D finite element-boundary element (FE-BE) model to analyse the effect of soil depth and shear speed. Sheng et al. [29] developed a similar model to predict ground surface vibrations. Bian et al. [30–32] investigated resonance of subgrade soil at the critical velocity using a 2.5D FE model, where Fourier transform was carried out in the spatial domain. Similar models were also developed to examine ground vibrations induced by train passing on multi-layered grounds [33,34]. Galvín et al. [35] considered two alternative models of a ballasted track on embankment. They developed a 2.5D model and the results showed that the model is capable of producing good estimations of the dynamic responses at low frequencies caused by the ballast and embankment. 2.5D FE models were also developed in other studies and the results showed that variations of stiffness and strain of the soft soil foundation are directly related to the train loads [36,37]. Track irregularity sometimes affects the dynamic response of the track and subgrade structure below the critical speed [38–40], Kouroussis et al. [41] discussed wheel-rail irregularities and concluded that wheel-rail type and contact conditions may have an impact on vibration. After that, Bian et al. [42] found that track irregular with smaller wavelengths cause high track and ground vibrations.

Although 2.5D FE models have been widely used to study the structural dynamics of high-speed railways systems, the assumption of a fixed longitudinal geometry is no longer valid under certain conditions. Thus, three-dimensional (3D) FE models were developed to overcome the limitations of 2.5D FE models. A 3D FE-BE model was developed to analyse the dynamic behaviour of the transition zone induced by the passing train [43]. Galvín et al. [44] developed a 3D multi-body FE-BE model to understand the characteristics of the soil affected by the track system. Connolly et al. [45] found that the material composition of the embankment affects the vibrational energy conductance of the track and surrounding soil by carrying out simulations using a 3D FE model. El Kacimi et al. [46] established a 3D FE model of vehicle coupled with multi-layered soil taking into account the material damping and non-linearity of the soil material. The results showed that the damping mode affects the track vibrations and prediction of the dynamic response of the vehicle body. Shan et al. [47] studied the dynamic responses of the subgrade transition section and found that the longer the transition section, the smaller the differences in the dynamic responses. The accuracy of the dynamic responses of the subgrade under moving constant loads was improved by accounting for non-linearities in the 3D FE model [48]. Gao et al. [49] developed a 3D track-subgrade interaction model to predict the soil dynamic responses. Varandas et al. [50] analysed the reasons behind the increase in settlement of the ballast layer and embankment in the transition zones by 3D simulations.

Although numerical models have been developed extensively to study the dynamic responses of subgrades, most of these studies are focused on single-line and half double-line subgrade models. Due to the fact that more than 90% of the high-speed railways in China are double-line, there is a critical need to examine the dynamic responses of subgrades under double-line high-speed railways. With the increase in high-speed train density, bidirectional running trains have become the basic operation mode of high-speed railways. To the best of the authors' knowledge, there are no studies concerning the dynamic response of subgrade subject to bidirectional running train loads. In addition, little is known on the effect of train speed on the dynamic behaviour of subgrade subject to these loads, which forms the motivation of this study.

In this study, a 3D FE model is developed to examine the dynamic responses of subgrade and the model is validated against experimental data in a previous study [51]. Simulations are carried out to determine the dynamic responses (vertical stress, displacement, velocity, and acceleration) of the subgrade subject to unidirectional and bidirectional moving constant loads at various train speeds (250, 300, and 360 km/h). The dynamic responses at three points on the subgrade surface

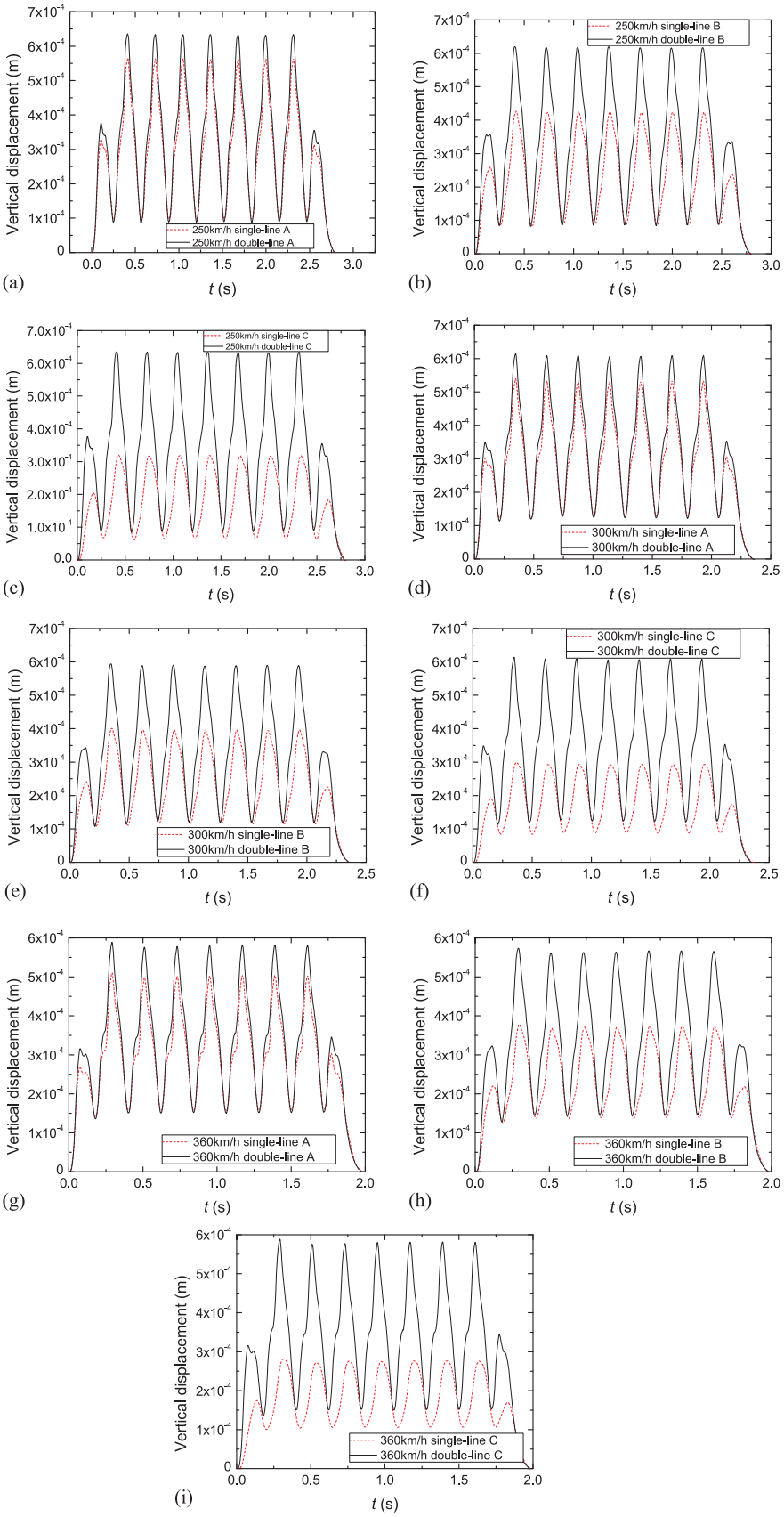

Fig. 6. Vertical displacement-time history curves at Point A, Point B, and Point C.

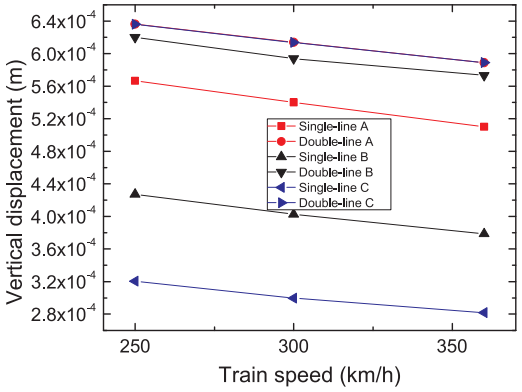

Fig. 7. Variation of the maximum vertical displacement with train speed.

(Point A, Point B, and Point C) obtained for different line patterns and train speeds are compared and the variations of the maximum vertical stress, displacement, velocity, and acceleration with train speed are presented for each observation point. The stress distributions at selected points along the subgrade surface and the variations of vertical stress along the soil depth for Point A and Point B are also studied and presented in this paper.

2. Dynamic 3D FE model of the double-line ballastless track-subgrade structure

2.1. Numerical model and simulation parameters

A 3D FE model was developed using ABAQUS software based on the prototype of a Beijing-Shanghai double-line low-embankment high-speed ballastless slab track railway (Fig. 1). The parameters were determined based on the design specifications of high-speed railways in China (TB10621-2014) [52]. The FE model of the double-line ballastless track-subgrade structure is shown in Fig. 2. CHN60 rail with a standard gauge of 1.435 m and 300-1a type fasteners with a spacing of 0.625 m were selected for the model. The width and thickness of the CRTS-II ballastless slab were 2.55 and 0.2 m, respectively. A cement asphalt mortar (CAM) layer was placed below the slab, with a width and thickness of 0.2 and 0.03 m, respectively. The trapezoidal cross section supporting layer with a width of 2.95–3.25 m and thickness of 0.3 m lies at the bottom of the track structure. The subgrade structure consists of a surface layer (thickness: 0.3 m), bottom layer (thickness: 2.4 m), and embankment layer (thickness: 2 m), with a surface width of 13.6 m and gradient of 1:1.5. The standard line spacing of the double-line railway was set as 5 m based on the specifications above. Since the energy transferred from the upper dynamic loads will be attenuated in the subgrade, the width of the sub-soil should not be too wide. Therefore, the width and depth of the foundation were set at 47.7 and 20 m, respectively. In order to accurately analyse the dynamic response of the model and consider the stress concentration in these local areas below the track structure, different element sizes were chosen to meet the computational convergence and the optimal element sizes were finally determined. For example, in order to study the stress concentration in the local area under the track structure, the element size was set to 0.14 m, while for other areas, the maximum element length was set to 0.5 m.

The rail was modelled using the Euler-Bernoulli beam element. The 300-1a type fasteners and the rail pads between the rail and slab can be treated as linear elastic components and therefore, they were modelled using spring-damper elements with a spring stiffness of 45 kN/mm and damping coefficient of 45,000 [53]. Eight-node hexahedral solid elements were used for the slab, CAM layer, supporting layer, subgrade, and foundation. The key simulation parameters are presented in Table 1. The Mohr-Coulomb model was used to simulate the constitutive relationship of the subgrade and foundation materials because the compressive yield strength values of these materials are significantly higher than the tensile yield strength values, and therefore, these materials are easily expanded by shear stresses. The linear elastic constitutive relationship was selected for concrete, steel, and other materials. To ensure continuity of the interface deformation, tie connection was used to ensure mutual contact between the layers under the slab. The bottom of the foundation was fixed and the four edges were surrounded by a semi-uniform viscoelastic artificial boundary, which reflects the propagation of actual waves in the foundation [54].

2.2. Rayleigh damping parameters

It is known that the damping coefficients of the subgrade and foundation have a significant effect on the vibration characteristics of the subgrade. In this study, Rayleigh damping was adopted for the 3D FE model:

$$\mathbf{C} = \alpha\mathbf{M} + \beta\mathbf{K}$$
$$\alpha = \frac{2\omega_i\omega_j}{\omega_i + \omega_j}\xi$$
$$\beta = \frac{2\xi}{\omega_i + \omega_j} \quad (1)$$

Here, **C**, **M**, and **K** represent the damping, mass, and stiffness matrices, respectively, α and β are the Rayleigh damping parameters, and ξ is the damping ratio. It should be noted that for numerical simulations, ω_i is always taken as the fundamental frequency of the model whereas ω_j is chosen from the higher-order vibration modes and has a significant contribution to the dynamic response.

The procedure used to determine the Rayleigh damping parameters is described as follows. Firstly, modal analysis was carried out for the FE model. The first 40 natural circular frequencies and the participation coefficients of the vertical formation at different frequencies were extracted to determine the fundamental frequency ω_i. Following this, ω_j was selected from the higher-order vibration modes and has a significant contribution to the dynamic response. It shall be noted that ω_j corresponds to the largest absolute value of the vertical formation participation coefficient. In this paper, w_i and w_j are 11.66 rad/s and 14.679 rad/s, respectively. The damping ratios ξ for the subgrade and ground are typically selected within a range of 0.03–0.05. In this study, the damping ratios of the surface layer of subgrade, bottom layer of subgrade, embankment layer, and ground were selected as 0.045, 0.039, 0.035, and 0.035, respectively. The values of the aforementioned parameters were inserted into Eq. (1) to determine the Rayleigh damping parameters (α and β) of the different structural layers. In this paper, the values of α for the subgrade surface, the subgrade bottom layer, the embankment layer and the ground are 0.585, 0.507, 0.455 and 0.455, respectively. The values of β for the subgrade surface, the road base layer, the embankment layer and the ground are 0.0034, 0.003, 0.003 and 0.003, respectively.

2.3. Simulation conditions

The 8-carriage CRH3 high-speed electrical multiple unit (EMU) train runs on a double-line high-speed railway with a bogie axle weight of 15 t and 32 wheels on each side. The numerical simulations were carried out for six moving constant load cases with three train speeds (250, 300, and 360 km/h) and two line patterns (unidirectional and bidirectional operations). The simulation cases are tabulated in Table 2. The dynamic responses were determined at three points on the subgrade surface (Point A, Point B, and Point C) within the intersection area of the FE model (Fig. 2). Point A is located at the subgrade surface underneath the left rail of the left line, Point B is located at the centre of the subgrade, and Point C is located at the subgrade surface underneath the right rail of the right line. In addition, several points were selected

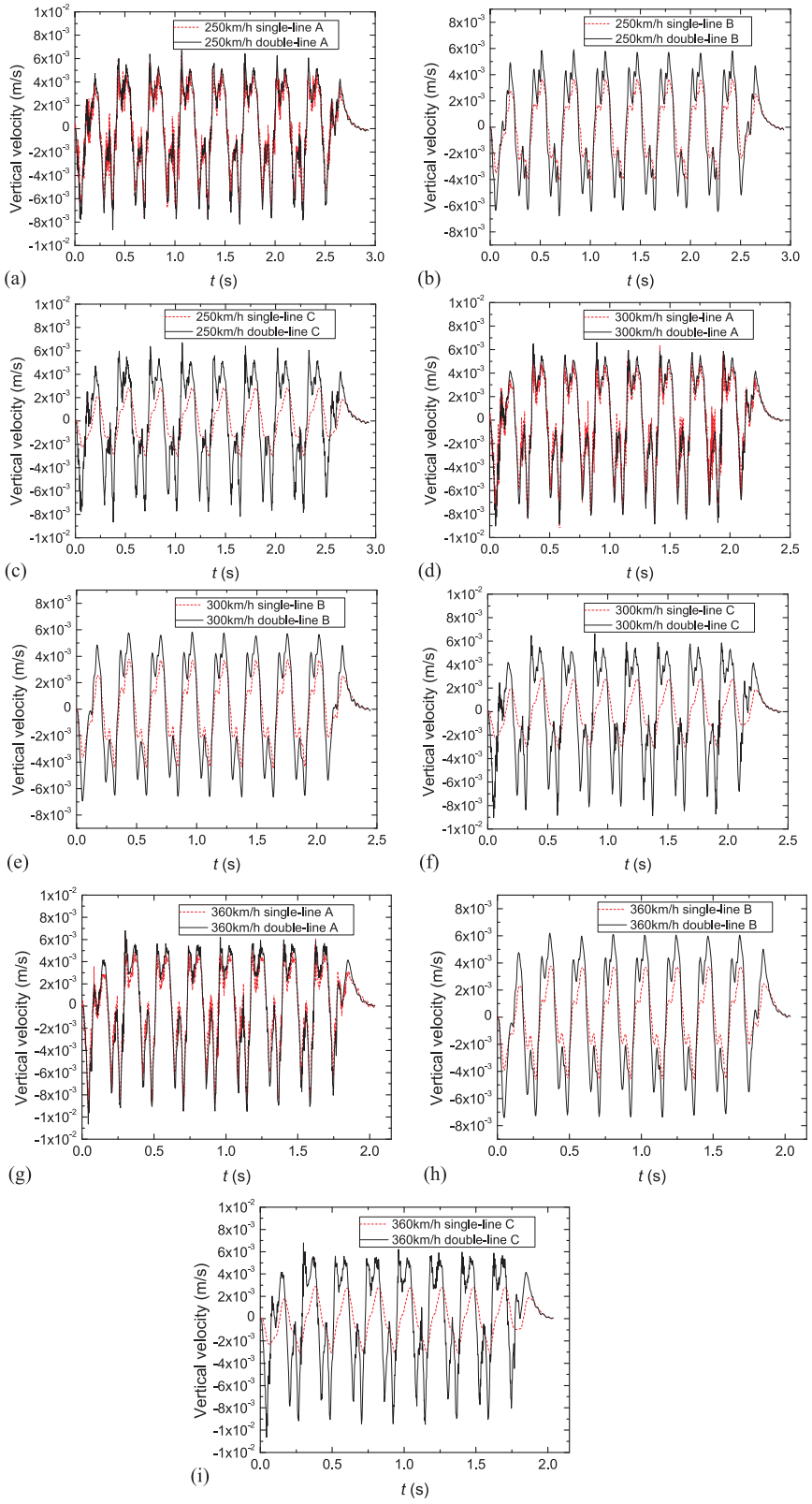

Fig. 8. Vertical velocity-time history curves at Point A, Point B, and Point C.

in order to analyse the stress distributions along the subgrade surface. Bidirectional moving constant loads at a speed of 360 km/h was chosen as the baseline operating condition. The vertical stresses along the soil depth projected from Point A were also studied in order to determine the attenuation of stress in the subgrade.

2.4. Validation of the model

In order to validate the feasibility of the 3D FE model, the simulation results were compared with those obtained from field test of a double-line high-speed railway and indoor test of a full-scale high-speed

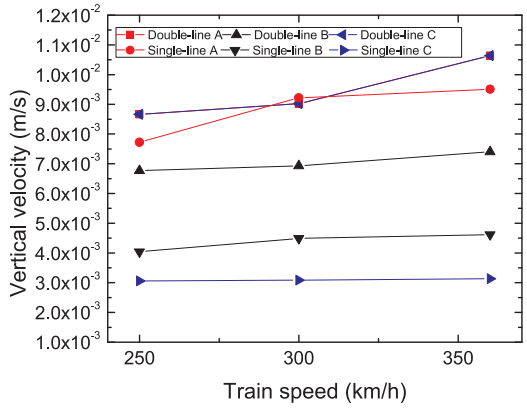

Fig. 9. Variation of the maximum vertical velocity with train speed.

railway physical model [51]. The following settings were used in the numerical simulations: (1) train speed: 330 km/h, (2) distance between the centres of the bogies: 17.375 m, (3) wheel base: 2.5 m, and (4) axle load: 14 t.

The vertical stresses at Point A obtained from numerical simulations were compared with those from field tests and indoor tests (Fig. 3). The maximum vertical stress obtained from the field tests, numerical simulations, and indoor tests are 14.5, 15.0, and 15.9 kPa, respectively. It can be observed that there is good agreement in the vertical stress-time history curves between the field tests, numerical simulations, and indoor tests, which validates the accuracy of the 3D FE model.

3. Dynamic responses of the subgrade for different train speeds and line patterns

3.1. Vertical stresses at Point A, Point B, and Point C

The vertical stress-time history curves for all operating conditions at Point A, Point B, and Point C are shown in Fig. 4. It can be seen that the vertical stress-time history curves have a distinctive, M pattern under moving constant loads, which are consistent with the results of Bian [51]. The positions of the load axles can be identified from the crests in the dynamic response of the subgrade surface.

At Point A (Fig. 4a, d, and g), the maximum vertical stress due to the dynamic loads decreases from 18.68 kPa (unidirectional operation) to 16.48 kPa (bidirectional operation) at a train speed of 360 km/h. The vertical stress under the rear bogie is higher than that under the front bogie for bidirectional operation, with a maximum difference of 2.5 kPa. Moreover, the maximum vertical stresses are also lower for bidirectional operation after the front bogie has left Point A, which indicates that stress redistribution occurs in the intersection area. At Point B (Fig. 4b, e, and h), the maximum compressive stress for bidirectional operation is 0.107 kPa, which is close to that for unidirectional operation. However, the stress interval at Point B is significantly smaller for unidirectional operation compared with that for bidirectional operation. At Point C (Fig. 4c, f, and i), the maximum vertical stress fluctuates around 50 kPa at different train speeds for unidirectional operation. The maximum vertical stress reduces to 16 and 14 kPa under the rear bogie and front bogie, respectively, for bidirectional operation. The dynamic response of the subgrade surface indicates that the moving constant loads is not simply a superposition of loads and stress redistribution occurs in the intersection area. This offers insight on designing the subgrade structure at the intersection area taking into account stress redistribution due to the long-term moving constant loads.

Fig. 5 shows the variation of maximum vertical stress with train speed. It can be seen that the maximum vertical stress at Point A increases by 6% and 2% for bidirectional and unidirectional operation, respectively, as the train speed increases from 250 to 360 km/h. The maximum vertical stress at Point B decreases from 2.05 kPa (unidirectional operation) to 1.14 kPa (bidirectional operation), which contrasts the increasing trend at Point A. At Point C, the maximum vertical stress increases at a higher rate for bidirectional operation, judging from the slope of the plot.

It shall be noted that Point A is located at the subgrade surface underneath the left rail of the left line, Point B is located at the centre of the subgrade surface, and Point C is located at the subgrade surface underneath the right rail of the right line. At Point A, the maximum vertical stress is lower for bidirectional operation compared with that for unidirectional operation. However, a different trend is observed for the vertical displacement. At Point B and Point C, the maximum vertical stresses are higher for bidirectional operation and likewise, the maximum vertical displacement shows a similar trend at these points.

The observed trend may be due to variations in the moving constant loads with time on the left track structure for unidirectional operation. In this case, the subgrade is subjected to eccentric dynamic loads in the left line. In bidirectional operation, the left and right track structures are both subjected to dynamic loads and therefore, the left and right regions of the subgrade both bear the effects of the dynamic loads transmitted along the soil depth. This leads to variations in the stress field of the subgrade surface, resulting in stress redistribution. Hence, the maximum vertical stress at Point A is lower whereas the maximum vertical stress at Point B is higher for bidirectional operation.

3.2. Vertical displacements at Point A, Point B, and Point C

The vertical displacement-time history curves at Point A, Point B, and Point C are shown in Fig. 6. Fig. 7 shows the relationship between the maximum vertical displacement and train speed and it can be observed that the maximum vertical displacements at these points are larger for bidirectional operation compared with those for unidirectional operation, which indicates that the subgrade sustains more external force in the former condition. It can be seen from Fig. 6a, d, and g that there is good agreement in the phase of the vertical displacement extreme values between unidirectional and bidirectional operations. However, the remaining sub-plots of Fig. 6 show a different trend, where the downward transmission of vibration energy is greater than the lateral transmission of vibration energy. It can be observed from Fig. 7 that the maximum vertical displacement decreases at all observation points as the train speed increases from 250 to 360 km/h. The maximum vertical displacement at Point C is 0.28 mm at 360 km/h for unidirectional operation. However, the maximum vertical displacement increases to 0.59 mm for bidirectional operation, which is 2.1 times the value obtained for unidirectional operation at the same train speed. The maximum displacement at Point A is 0.59 mm at 360 km/h for bidirectional operation, which is only 1.16 times the value (0.51 mm) obtained for unidirectional operation.

At Point A, the vertical displacement field has a superposed effect due to the asymmetric loads during bidirectional operation, which differs from the eccentric dynamic loads during unidirectional operation. Thus, the maximum vertical displacement of the subgrade is larger under unidirectional moving constant loads.

Even though the vertical displacement of the subgrade subject to moving constant loads is presented as instantaneous deformation, it is perceived that this parameter should be related to the loading time because it is a dynamic response. This is because regardless whether the applied load is a simulation of the moving constant load or the actual train load, these dynamic loads are transmitted to the railway track and subgrade structure as the train passes by each node. At a train speed of 250 km/h, the time available for the applied compressive load to contact a particular node is longer compared with that at a train speed of 360 km/h. At higher train speeds, the time available for the applied train load to contact each node is reduced, which leads to smaller displacements at Point A, Point B, and Point C. Thus, the vertical

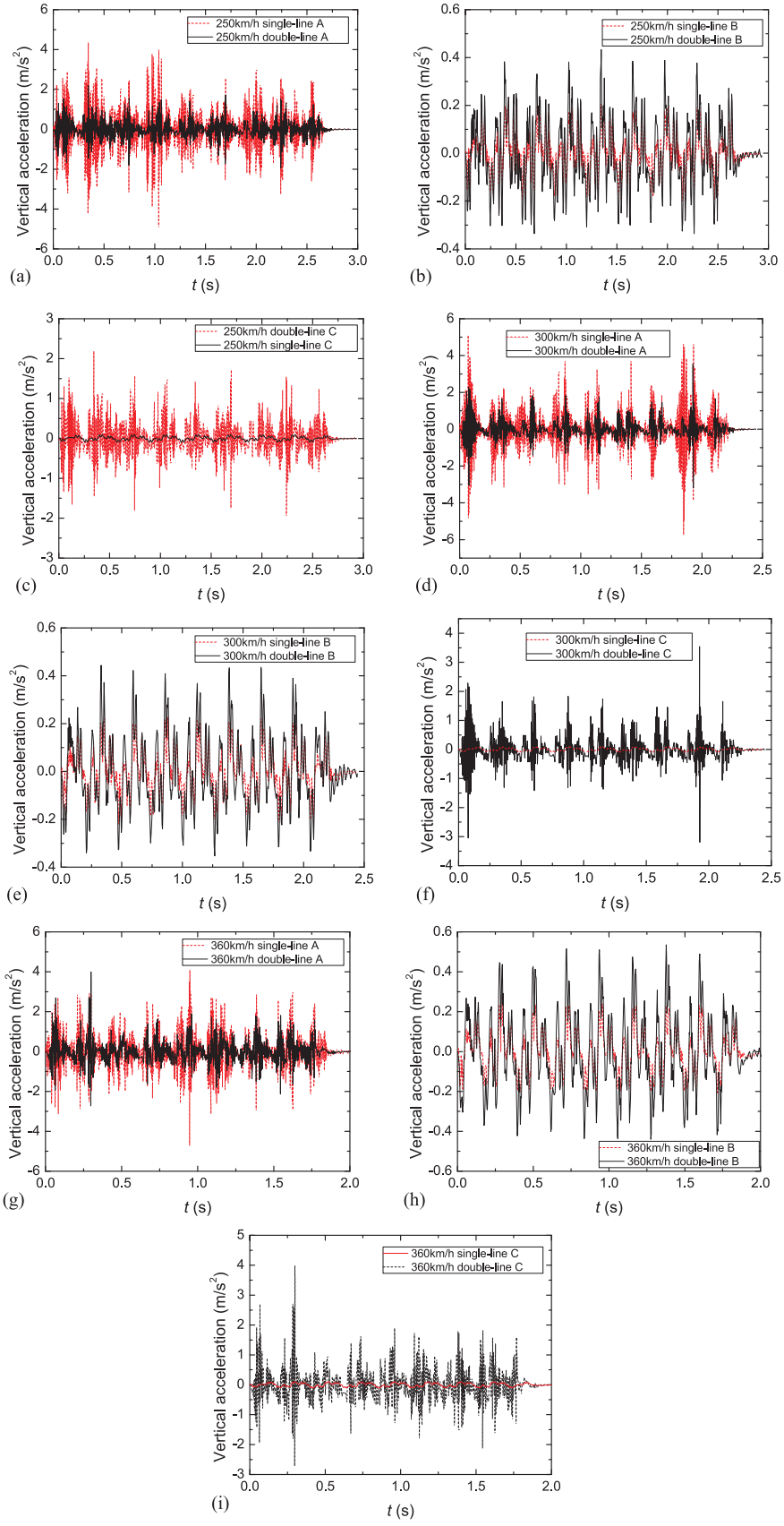

Fig. 10. Vertical acceleration-time history curves at Point A, Point B, and Point C.

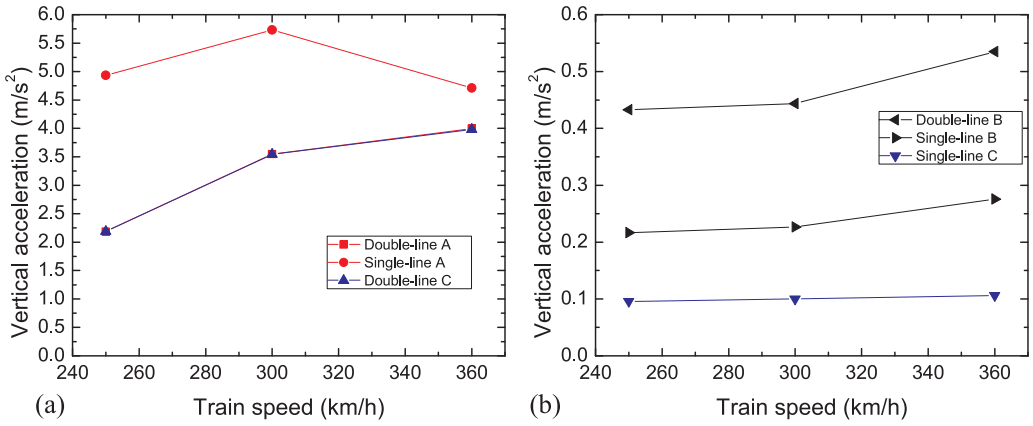

Fig. 11. Variation of the maximum vertical acceleration with train speed.

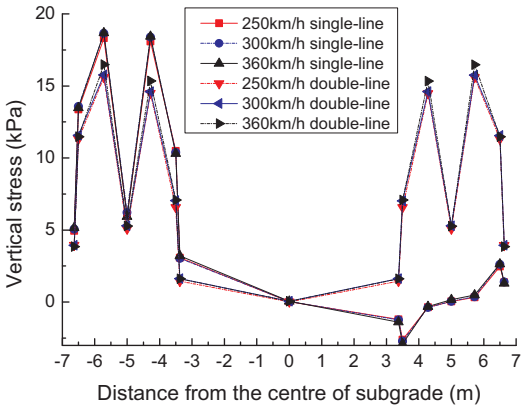

Fig. 12. Vertical stress distributions along selected points on the subgrade surface.

displacement decreases as the train speed increases, as shown in Fig. 7.

3.3. Vertical velocities at Point A, Point B, and Point C

The vertical velocities obtained from the numerical simulations are plotted in Fig. 8 for three train speeds and two line patterns. The absolute maximum vertical velocities were determined based on the results, as shown in Fig. 9. It can be deduced from Fig. 8 that the inflection points of the vertical velocity-time history curves are mainly controlled by the bogie loads rather than the wheel loads where the vibration energy is transmitted from top to bottom. The vertical velocities are higher at Point A, Point B, and Point C for bidirectional operation. The absolute maximum vertical velocities at Point A are 10.64 and 9.50 mm/s for bidirectional and unidirectional operation, respectively, at a train speed of 360 km/h (Fig. 9). The results also indicate that the absolute maximum vertical velocity slightly increases as the train speed increases from 250 to 360 km/h at all three observation points.

3.4. Vertical accelerations at Point A, Point B, and Point C

The vertical acceleration-time history curves at Point A, Point B, and Point C induced by the high-speed EMU trains in different operating conditions are shown in Fig. 10. It is evident that the vertical acceleration fluctuates greatly at these observation points. The maximum vertical accelerations at Point A (Fig. 10a, d, and g) are 4.7 and 4.0 m/s^2 for bidirectional and unidirectional operation, respectively, at a train speed of 360 km/h. The maximum vertical acceleration occurs at the bogie front of the second carriage and bogie rear of the fourth carriage. By analysing the vertical accelerations at Point B (centre of subgrade) under different operating conditions (Fig. 10b, e, and h), the maximum vertical acceleration is found to be 0.54 m/s^2 for bidirectional operation, which is twice the value for unidirectional operation. The vibrations at Point B are more severe for bidirectional operation compared with those for unidirectional operation. The maximum vertical acceleration at Point C is 0.11 m/s^2 which occurs at the bogie front of the second carriage for unidirectional operation, which is significantly lower than that (3.98 m/s^2) for the same bogie under bidirectional operation (Fig. 10c, f, and i). It can be deduced from Fig. 11 that there is a positive correlation between the maximum vertical acceleration and train speed at Point B and Point C.

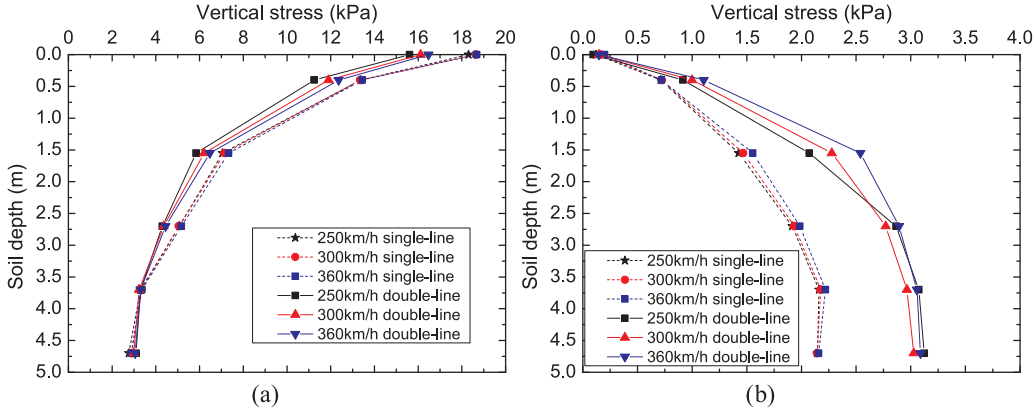

Fig. 13. Variation of vertical stress along the soil depth of the subgrade at (a) Point A and (b) Point B.

3.5. Vertical stress distributions of the subgrade surface

Fig. 12 shows the vertical stress distributions along selected points on the subgrade surface, which provides insight on the plane stress distributions. It is apparent that the vertical stress fluctuates at different points along the subgrade surface for different train speeds (250, 300, and 360 km/h) and line patterns (unidirectional and bidirectional operations). At the subgrade surface, the vertical stresses under the rails are significantly higher compared with those under the edge of the supporting layer and track centre. The maximum vertical stresses on the left side of the supporting layer and under the right rail for unidirectional operation are higher than those for bidirectional operation by 1.31 and 3.79 kPa, respectively. The stress redistribution can be assessed by examining the changes in the load-carrying capability of the subgrade structure. The vertical stress distribution of the subgrade structure is highly uneven when the moving constant loads are imposed on the left track for bidirectional operation, which is indeed expected due to the non-uniform internal force distribution of the subgrade.

3.6. Stress attenuation in the subgrade

The stresses under the track structure induced by the high-speed EMU trains are one of the critical factors that need to be considered in high-speed railway designs. Fig. 13 shows the variation of vertical stress along the soil depth at Point A and Point B. The soil depth is measured from the centre of the subgrade surface layer to the bottom of the embankment layer. It is apparent from Fig. 13a that the vertical stress attenuates gradually along the soil depth and the attenuation of vertical stress is more marked for bidirectional operation, indicating that the subgrade surface layer absorbs more of the vibration energy when the 8-carriage EMU trains run in opposite directions. In addition, the vertical stresses tend to be even in the embankment layer at different train speeds, since the vertical stresses are nearly coincident at a soil depth of more than 4.5 m. However, a different trend is observed for Point B (Fig. 13b), where the vertical stress is 3.09 kPa at the bottom of the embankment layer (train speed: 360 km/h, line pattern: bidirectional operation), which is 1.43 times higher than that for unidirectional operation (2.16 kPa). It can be deduced that the vertical stress at the centre of the subgrade is influenced by the bidirectional moving constant loads. The vertical stress at each point at the centre of the subgrade is not merely a superposition of the bidirectional moving constant loads, which is consistent with the previous results.

4. Conclusions

A 3D FE model was developed in this study in order to examine the effects of train speed (250, 300, and 360 km/h) and line patterns (unidirectional and bidirectional operations) on the dynamic responses of subgrade subject to high-speed moving constant loads. The following conclusions are drawn based on the findings:

(1) The maximum vertical stress increases with an increase in train speed for both unidirectional and bidirectional operations. The maximum vertical stress of the subgrade increases by 6% and 2% for bidirectional and unidirectional operation, respectively, as the train speed increases from 250 to 360 km/h. However, the maximum vertical stresses are generally lower for bidirectional operation.
(2) The vertical displacements are higher at all observation points (Point A, Point B, and Point C) for bidirectional operation, indicating that the subgrade structure sustains more external force.
(3) The vertical velocity slightly increases as the train speed increases from 250 to 360 km/h. The vertical velocity-time history curves are mainly controlled by the bogie loads, rather than the wheel loads. The absolute maximum vertical velocities of the subgrade are 10.64 and 9.50 mm/s for bidirectional and unidirectional operation, respectively, at 360 km/h.
(4) The maximum vertical acceleration at Point B is 0.54 m/s^2 for bidirectional operation, which is twice the value for unidirectional operation.
(5) The vibrations at Point B are more severe for bidirectional operation compared with those for unidirectional operation.
(6) At the subgrade surface, the vertical stresses are maximum under the rails and the stress distributions are asymmetric for bidirectional operation.
(7) The vertical stress attenuates along the soil depth at Point A and the vertical stress attenuation is more pronounced under bidirectional operation. However, a different trend is observed at Point B, where the vertical stress amplifies along the soil depth. The vertical stresses at Point A and Point B tend to be close to one another with an increase in soil depth such that the values are nearly coincident in the embankment layer within the range of train speeds investigated in this study.

Acknowledgments

The work in this paper is supported by the National Basic Research Program of China (973 Program) (Project No. 2014CB049100). The financial support is gratefully acknowledged.

References

[1] Jones DV, Petyt M. Ground vibration in the vicinity of a strip load: a two-dimensional half-space model. J Sound Vib 1991;147(1):155–66.
[2] Krylov VV. Generation of ground vibrations by superfast trains. Appl Acoust 1995;44(2):149–64.
[3] Dieterman HA, Metrikine AV. Equivalent stiffness of a half-space interacting with a beam. critical velocities of a moving load along the beam. Eur J Mech A Solid 1996;15(1):67–90.
[4] Grundmann H, Lieb M, Trommer E. The response of a layered half-space to traffic loads moving along its surface. Arch Appl Mech 1999;69(1):55–67.
[5] Hung HH, Yang YB. Elastic waves in visco-elastic half-space generated by various vehicle loads. Soil Dyn Earthq Eng 2001;21(1):1–17.
[6] Alshaikh IA, Turhan D, Mengi Y. Two-dimensional transient wave propagation in viscoelastic layered media. J Sound Vib 2001;244(5):837–58.
[7] Bitzenbauer J, Dinkel J. Dynamic interaction between a moving vehicle and an infinite structure excited by irregularities – fourier transforms solution. Arch Appl Mech 2002;72(2):199–211.
[8] Kaynia AM, Madshus C, Zackrisson P. Ground vibration from high-speed trains: prediction and countermeasure. J Geotech Geoenviron 2000;126:531–7.
[9] Takemiya H, Satonaka S, Xie WP. Train track-ground dynamics due to high speed moving source and ground vibration transmission. P Jpn Soc Civil Eng 2001;682:299–309.
[10] Sheng X, Jones CJC, Thompson DJ. A theoretical model for ground vibration from trains generated by vertical track irregularities. J Sound Vib 2004;272(3–5):937–65.
[11] Schwarz P. Laier. Final experiment report on Günzburg-Augsburg extension line. TU Munich, 1991.
[12] Okumura Y, Kuno K. Statistical analysis of field data of railway noise and vibration collected in an urban area. Appl Acoust 1991;33(4):263–80.
[13] Madshus C, Bessason B, Hårvik L. Prediction model for low frequency vibration from high speed railways on soft ground. J Sound Vib 1996;193(1):195–203.
[14] Madshus C, Kaynia AM. High-speed railway lines on soft ground: dynamic behaviour at critical train speed. J Sound Vib 2000;231(3):689–701.
[15] Turunen-Rise IH, Brekke A, Harvik L, et al. Vibration in dwellings from road and rail traffic — Part I: a new Norwegian measurement standard and classification system. Appl Acoust 2003;64(1):71–87.
[16] Bahrekazemi M, Bodare A. Effects of Lime-Cement Soil Stabilization against Train Induced Ground Vibrations. 2003.
[17] Takemiya H. Substructure simulation of inhomogeneous track and layered ground dynamic interaction under train passage. J Eng Mech-ASCE 2005;131(7):699–711.
[18] Momoya Y, Sekine E, Tatsuoka F. Deformation characteristics of railway roadbed and subgrade under moving-wheel load. Soil Found 2005;45(4):99–118.
[19] Brown SF, Brodrick BV, Thom NH, et al. The Nottingham railway test facility, UK. P I Civil Eng Transp 2007;160(2):59–65.
[20] Al Shaer A, Duhamel D, Sab K, et al. Experimental settlement and dynamic behavior of a portion of ballasted railway track under high speed trains. J Sound Vib 2008;316(1):211–33.
[21] Ishikawa T, Sekine E, Miura S. Cyclic deformation of granular material subjected to moving-wheel loads. Can Geotech J 2011;48(5):691–703.
[22] Jiang HG, Bian XC, Cheng C, et al. Simulating train moving loads in physical model testing of railway infrastructure and its numerical calibration. Acta Geotech 2016;11(2):231–42.
[23] Balendra T, Chua KH, Lo KW, Lee S. Steady-state vibration of subway-soil-building

system. J Eng Mech ASCE 1989;115(1):145–62.
[24] Takemiya H, Sukeyasu Y. Transient response of rigid strip foundations on a half-space/stratum soil due to impulsive loads. Comput Methods Adv Geomech 1994;2:993–8.
[25] Ekevid T, Li MXD, Wiberg NE. Adaptive FEA of wave propagation induced by high-speed trains. Comput Struct 2001;79(29):2693–704.
[26] Hanazato T, Ugai K, Mori M, Sakaguchi R. Three-dimensional analysis of traffic-induced ground vibrations. J Geotech Eng 1991;117:1133–51.
[27] Yang YB, Hung HH. A 2.5 D finite/infinite element approach for modelling visco-elastic bodies subjected to moving loads. Int J Numer Methods Eng 2001;51(11):1317–36.
[28] Yang YB, Hung HH, Chang DW. Train-induced wave propagation in layered soils using finite/infinite element simulation. Soil Dyn Earthq Eng 2003;23(4):263–78.
[29] Sheng X, Jones CJC, Thompson DJ. Prediction of ground vibration from trains using the wavenumber finite and boundary element methods. J Sound Vib 2006;293(3):575–86.
[30] Bian XC, Chen YM, Hu T. Numerical simulation of high-speed train induced ground vibrations using 2.5 D finite element approach. Sci China Ser E Ph Mech Astron 2008;51(6):632–50.
[31] Bian XC, Chao C, Jin WF, et al. A 2.5 D finite element approach for predicting ground vibrations generated by vertical track irregularities. J Zhejiang Univ Sci A 2011;12(12):885–94.
[32] Bian XC, Jin WF, Jiang HG. Ground-borne vibrations due to dynamic loadings from moving trains in subway tunnels. J Zhejiang Univ Sci A 2012;13(11):870–6.
[33] François S, Schevenels M, Galvín P, et al. A 2.5 D coupled FE–BE methodology for the dynamic interaction between longitudinally invariant structures and a layered halfspace. Comput Method Appl M 2010;199(23):1536–48.
[34] Gao GY, Chen QS, He JF, et al. Investigation of ground vibration due to trains moving on saturated multi-layered ground by 2.5 D finite element method. Soil Dyn Earthq Eng 2012;40:87–98.
[35] Galvín P, François S, Schevenels M, et al. A 2.5 D coupled FE-BE model for the prediction of railway induced vibrations. Soil Dyn Earthq Eng 2010;30(12):1500–12.
[36] Costa PA, Calçada R, Cardoso AS, et al. Influence of soil non-linearity on the dynamic response of high-speed railway tracks. Soil Dyn Earthq Eng 2010;30(4):221–35.
[37] Costa PA, Calçada R, Cardoso AS. Track–ground vibrations induced by railway traffic: in-situ measurements and validation of a 2.5 D FEM-BEM model. Soil Dyn Earthq Eng 2012;32(1):111–28.
[38] Zhai W, Wang K, Cai C. Fundamentals of vehicle–track coupled dynamics. Veh Syst Dyn 2009;47(11):1349–76.
[39] Hung HH, Chen GH, Yang YB. Effect of railway roughness on soil vibrations due to moving trains by 2.5 D finite/infinite element approach. Eng Struct 2013;57:254–66.
[40] Germonpré M, Degrande G, Lombaert G. A study of modelling simplifications in ground vibration predictions for railway traffic at grade. J Sound Vib 2017;406:208–23.
[41] Kouroussis G, Connolly DP, Verlinden O. Railway-induced ground vibrations–a review of vehicle effects. Int J Rail Transp 2014;2(2):69–110.
[42] Bian X, Jiang H, Chang C, et al. Track and ground vibrations generated by high-speed train running on ballastless railway with excitation of vertical track irregularities. Soil Dyn Earthq Eng 2015;76:29–43.
[43] Galvín P, Romero A, Domínguez J. Fully three-dimensional analysis of high-speed train–track–soil-structure dynamic interaction. J Sound Vib 2010;329(24):5147–63.
[44] Galvín P, Romero A, Dominguez J. Vibrations induced by HST passage on ballast and non-ballast tracks. Soil Dyn Earthq Eng 2010;30(9):862–73.
[45] Connolly D, Giannopoulos A, Forde MC. Numerical modelling of ground borne vibrations from high speed rail lines on embankments. Soil Dyn Earthq Eng 2013;46:13–9.
[46] El Kacimi A, Woodward PK, Laghrouche O, et al. Time domain 3D finite element modelling of train-induced vibration at high speed. Comput Struct 2013;118:66–73.
[47] Shan Y, Albers B, Savidis SA. Influence of different transition zones on the dynamic response of track–subgrade systems. Comput Geotech 2013;48:21–8.
[48] Correia AG, Cunha J. Analysis of nonlinear soil modelling in the subgrade and rail track responses under HST. Transp Transp Geotech 2014;1(4):147–56.
[49] Gao Y, Huang H, Ho CL, et al. Field validation of a three-dimensional dynamic track-subgrade interaction model. Proc Inst Mech Eng F J Rapid 2016:1–14.
[50] Varandas JN, Hölscher P, Silva MAG. Three-dimensional track-ballast interaction model for the study of a culvert transition. Soil Dyn Earthq Eng 2016;89:116–27.
[51] Bian XC, Jiang HG, Cheng C, et al. Full-scale model testing on a ballastless high-speed railway under simulated train moving loads. Soil Dyn Earthq Eng 2014;66:368–84.
[52] TB 10621-2014. Code for design on subgrade of China's high-speed railway. (in Chinese); 2014.
[53] Gao G, Chen J, Song J. et al. Field measurement and analysis of ground vibration induced by high-speed train. In: Proceedings of the International Symposium on Environmental Vibration and Transportation Geodynamics. 2016. p. 119–132.
[54] Chen J, Zhou GX, Zhou Y, Zhang FL. Influences of different boundary conditions on three-dimensional structure of ballastless track-subgrade under exogenous excitation. In: Proceedings of the 6th Asian-Pacific symposium on structural reliability and its applications, vol. 6. 2016. p. 699–703.